Mineralogy and Petrology (2023) 117:761–774
https://doi.org/10.1007/s00710-023-00837-y

RESEARCH

Mallestigite, $Pb_3Sb(SO_4)(AsO_4)(OH)_6{\cdot}3H_2O$, from the type locality – new data, crystal structure, and structural relationships

Kurt Mereiter[1] · Franz Walter[2] · Hans-Peter Bojar[2]

Received: 4 April 2023 / Accepted: 19 June 2023 / Published online: 11 September 2023

Abstract
A report of the supergene mineral mallestigite, $Pb_3Sb^{5+}(SO_4)(AsO_4)(OH)_6{\cdot}3H_2O$, from the type locality Neufinkenstein-Grabanz district, Mallestiger Mittagskogel, Carinthia, Austria, is given in order to close gaps that have been left open since its first description. At the type locality, the dump of an abandoned small copper-lead-zinc mine, the mineral occurs frequently in up to ~2 mm long clear colourless idiomorphic hexagonal prisms {100} terminated by the bipyramid {101}. Details of the occurrence, paragenesis, physical properties, a FTIR spectrum and X-ray powder diffraction data are reported. Chemical analysis in a scanning electron microscope in conjunction with a crystal structure analysis gave the empirical formula $Pb_{3.02}Sb_{1.06}(SO_4)_{0.96}(AsO_4)_{0.97}(OH)_6{\cdot}3H_2O$. An ab-initio crystal structure determination with CCD diffractometer data, Mo$K\alpha$ radiation, and a nearly untwinned crystal proved that mallestigite is hexagonal, space group $P6_3$, $a=8.9326(4)$, $c=11.1044(5)$ Å, $V=767.33(8)$ Å^3, $Z=2$, and gave a final $R1=0.0184$ for 1632 independent reflections with $I>2\sigma(I)$. Mallestigite belongs to the fleischerite group. The structure is built up from $[Sb^{5+}(OH)_6]^{1-}$ octahedra which are linked by triplets of edge-sharing Pb^{2+} into chains $[Pb_3Sb(OH)_6]^{5+}$ extending along a 6_3 axis. Each three of such chains are bridged by triplets of H_2O and by rows of SO_4^{2-} and AsO_4^{3-} tetrahedra alternating along a 3-fold axis and showing very different links to the Pb atom. Pb^{2+} is in a strongly distorted one-sided [9]-coordination by O atoms that makes the structure clearly hemimorphic. Structural relationships to the fleischerite group minerals schaurteite, genplesite, despujolsite and fleischerite as well as to synthetic $Ba_3Sn^{4+}(SeO_4)_2(OH)_6{\cdot}3H_2O$ are outlined and changes in the space group symmetry of despujolsite ($P\bar{6}2c \rightarrow P6_3/mmc$) and fleischerite ($P\bar{6}2c \rightarrow P6_3$) are proposed.

Keywords Mallestigite · Fleischerite group · Mineral description · Crystal structure · Structural relationships · Mallestiger Mittagskogel

Introduction

Mallestigite was reported as a new mineral (IMA 1996-043) from the ore dump of a former copper-lead-zinc mine, which is located on Mallestiger Mittagskogel mountain, Carinthia, Austria. Brief reports about the mineral and its properties were subsequently published by Sima et al. (1996) and Sima (1998). But, due to issues regarding crystallography a full report of the mineral was postponed. Since then, the mineral was reported from further occurrences in Tyrol and Styria, Austria (Poeverlein and Gröbner 2007; Walter et al. 2016), Northeastern Italy (Giarduz et al. 2015), Spain (Rewitzer et al. 2020) and as a weathering product from a slag dump near Goslar, Germany (Schnorrer 2003). The present paper aims to give an evaluation of the mineral from the type locality including a new structure determination, and to lay out structural relationships to related minerals and synthetic material investigated in recent years.

Occurrence and paragenesis

The type locality of mallestigite is an ore dump of a small abandoned copper-lead-zinc mine, located ~1195 m above sea level, ~1 km NW of the Mallestiger Mittagskogel peak, Karawanken range, in Carinthia, Austria (46°31'56.7'' N,

Editorial handling: L. Bindi.

✉ Kurt Mereiter
kurt.mereiter@tuwien.ac.at

[1] Institute of Chemical Technologies and Analytics, Research Unit of Structural Chemistry, TU Wien, Getreidemarkt 9/164-SC, Vienna A-1060, Austria

[2] Centre of Natural History, Universalmuseum Joanneum, Weinzöttlstraße 16, Graz A-8045, Austria

13°52'21.7'' E). This mine belongs to the polymetallic sulfide ore district of western South-Karawanken (Weber 1997; IRIS 2023) comprising small former sediment-hosted copper mines and prospects that operated mainly in the 15th–16th and in the 19th century in an approximately 10 km East-West extending area south of Finkenstein near Villach, Carinthia, Austria (Puttner 1994). They all seem to be bound to strips of E-W extending limestones in schist or sandstone strata of Palaeozoic age, but geologic and genetic details are still unclear (Weber 1997; IRIS 2023). The small orebodies of interest were stratiform or impregnations and carried fahlore, galena, sphalerite and secondary minerals like malachite and azurite. One of these mining places is the "Neufinkenstein-Grabanz" district and to this district does the type locality of mallestigite belong, known under the historic names "Segen Gottes" mining claim and "Glückauf" mining tunnel (Puttner 1994). Here fahlore, chalcopyrite, galena and sphalerite, with baryte as gangue, and secondary malachite were mined from a zone near the tectonic contact between Palaeozoic and lower Triassic formations (Canaval 1926; Puttner 1994, 1995; Weber 1997; IRIS 2023). The raw ore mined in the 1880s was collected on an ore dump of ~ 60 t that was not recovered because of non-profitability. This ore dump was since exposed to weathering in a humid continental climate with snow in winter and warm wet summers.

The mineral is found in narrow fractures and cavities of gangue and ore together with primary sulfides and secondary minerals. Fahlore – zoned, chemically inhomogeneous crystals of tennantite/tetrahedrite-(Zn) solid solutions with Sb/As ratios varying from 0.07 to 4.7 (for details see Taucher 1998) – is typically nearby. Mallestigite is found as idiomorphic to hypidiomorphic crystals up to 2 mm in length and 0.4 mm in thickness (Fig. 1). It may be confused with quartz or mimetite in its common hexagonal prismatic habit. It is also forming radial aggregates with diameters up to 3 mm. The mineral may have formed during weathering of the primary ore minerals galena and fahlore in the over 100 years old raw ore dump though oxidized Cu ore was once mined, too (Puttner 1994). It is associated with the sulfates anglesite, $PbSO_4$, brochantite, $Cu_4(SO_4)(OH)_6$, langite, $Cu_4(SO_4)(OH)_6{\cdot}2H_2O$, linarite, $PbCu(SO_4)(OH)_2$ and the rare arsenate schultenite, $Pb(HAsO_4)$. More than 60 further primary and secondary minerals have been reported from this site in the course of time, mainly sulfates, arsenates and carbonates of Cu, Pb, Zn, and among them theisite, $Cu_5Zn_5(AsO_4,SbO_4)_2(OH)_{14}$, and camérolaite, $Cu_6Al_3(OH)_{18}(H_2O)_2[Sb(OH)_6](SO_4)$, as two further Sb-bearing species apart from mallestigite. A list of the currently known minerals from this location has been presented in the supplementary materials together with corresponding references. Type specimens of mallestigite are deposited in the collections of the Centre of Natural History, Universalmuseum Joanneum, Weinzöttlstraße 16, A-8045 Graz, Austria, catalogue numbers 80.147 (holotype) and 86.348–86.350 (cotypes). The present investigation was based on holotype material except for Fig. 1.

Fig. 1 Typical crystals of mallestigite (cotype 86.350) on corroded quartz and weathered ore. Photograph Hans-Peter Bojar

Analytical characterization

Physical properties

Crystals of mallestigite from the type locality are transparent to translucent. They are colourless with adamantine lustre and give a white streak. The mineral is brittle with splintery fracture, no cleavage was observed. It does not fluoresce in ultraviolet radiation. Mallestigite has a simple morphology: hexagonal prism {100} elongated parallel [001] and terminated by the hexagonal dipyramid {101} (Fig. 1). Morphological twinning was not detected, but twinning by merohedry with (001) and (110) as twin planes was observed via X-ray investigations.

Optically, mallestigite is uniaxial positive, non-pleochroic and indices of refraction ($\lambda = 589$ nm) are $n_\omega = 1.760(4)$ and $n_\varepsilon = 1.801(4)$ according to measurements on a spindle stage using the λ-T-variation method. Mass density was not measured because it exceeded that of the Clerici solution and the sample amount was too small for pyknometry. The calculated mass density is 4.91 g cm^{-3} for the chemical formula $Pb_3Sb(SO_4)(AsO_4)(OH)_6{\cdot}3H_2O$ and the unit cell dimensions given below. Micro-indentation hardness measurements, using a microhardness tester, gave $VHN_{10} = 176$. This corresponds approximately to Mohs hardness of 4.

FTIR examinations were performed on a PerkinElmer Spectrum 100 instrument which was equipped with a

diamond universal attenuated total reflectance (ATR) sampling accessory. The same powder of mallestigite was used for PXRD and FTIR analytics. The spectrum represents the sum of 20 scans from 4000 to 500 cm^{-1} with a resolution of 2 cm^{-1}. No ATR correction was performed. Absorption bands in the IR spectrum of mallestigite (Fig. 2) and their tentative assignments are (cm^{-1}; s – strong band, sh – shoulder): ~3400sh, 3201, 2812 (O-H stretching vibrations); 2317 (overtone or combination modes); 1630 (H-O-H bending vibrations); 1216, 1117s, 1067sh, 1037s (asymmetric stretching vibrations of SO_4^{2-}); 964 (symmetric stretching vibrations of SO_4^{2-}); 798s (stretching vibrations of AsO_4^{3-}); 669sh, 616, 585s (unassigned). The spectrum and all bands are in good accordance with the two mallestigite spectra reported by Chukanov (2014).

Chemical composition

A mallestigite crystal was placed in a cylindrical brass sample holder and polished to a surface quality of 1 µm and coated with carbon. Chemical analyses were undertaken on a Jeol 6610 LV scanning electron microscope equipped with Oxford wavelength-dispersive spectrometers and an Oxford energy-dispersive detector. An accelerating voltage of 20 kV and a beam current of only 2 nA was used because mallestigite is very unstable at vacuum and under the electron microbeam. Moreover, the beam was rasterized on an area of 8 to 12 µm to reduce sample damage. Beside Pb, Sb, S and As, no other elements with an atomic number higher than 11 were detected in the energy-dispersive spectra. Following reference materials were used for quantification of the wavelength-dispersive analyses: PbS (galena) for Pb and S, GaAs for As, and Sb_2Te_3 for Sb. Data reduction was performed with the PAP routine (Pouchou and Pichoir 1991) as implemented in the INCA software of Oxford Instruments and element counts were normalized to 11 O atoms giving element proportions Pb:Sb:As:S of 3.03:1.08:0.99:0.93 (spot 1) and 3.02:1.04:0.93:1.02 (spot 2) with mean values of 3.02:1.06:0.96:0.97 and a sum of 6.01 atoms. The empirical formula of mallestigite is $Pb_{3.02}Sb_{1.06}(SO_4)_{0.96}(AsO_4)_{0.97}(OH)_6{\cdot}3H_2O$, where the OH and H_2O content is based on the crystal structure determination, giving the idealized chemical formula $Pb_3Sb(SO_4)(AsO_4)(OH)_6{\cdot}3H_2O$ subsequently applied. Chukanov (2014; pp 1174–1175) reported for a sample of mallestigite from the type locality a small amount of 0.1 SiO_4 replacing AsO_4. Giarduz et al. (2015) gave for mallestigite from Monte Avanza, Italy, the approximate chemical formula $Pb_{3.3}Sb_{1.2}(S_{0.9}O_4)(As_{1.2}O_4)(OH)_6{\cdot}3H_2O$.

Powder X-ray diffraction

Powder X-ray diffraction data for mallestigite from the type locality were obtained at 293 K using a Bruker D8 diffractometer with Cu*K*α radiation, an auto-divergence slit and a Lynxeye detector. The finely ground sample was placed on a low-background silicon specimen support, homogeneously distributed with a drop of ethanol, and was spun during measurement. Unit cell parameters were derived by Rietveld refinement with fundamental parameters using TOPAS 4.2 software (Bruker 2009) and the structural data of the single-crystal structure determination (see below; atomic coordinates fixed, U_{iso} of Pb, Sb, As, and S optimized). The dimensions of the hexagonal unit cell were found as $a = 8.9390(2)$ Å, $c = 11.1007(3)$ Å and $V = 768.18(3)$ Å^3, in good agreement with those obtained from the single-crystal study. When the sample was pressed with a glass slide, intensities of *h*00 reflections became texture enhanced. This appears to be in agreement with the observed morphology of mallestigite crystals and suggests that (100) is a cleavage plane. A comparison of the measured and calculated X-ray powder patterns is presented in Fig. 3. The measured pattern includes background as measured, the calculated pattern is background-free, and a difference curve measured minus Rietveld-fit intensities is shown below. $R_{wp} = 0.029$ and $R_{Bragg} = 0.024$

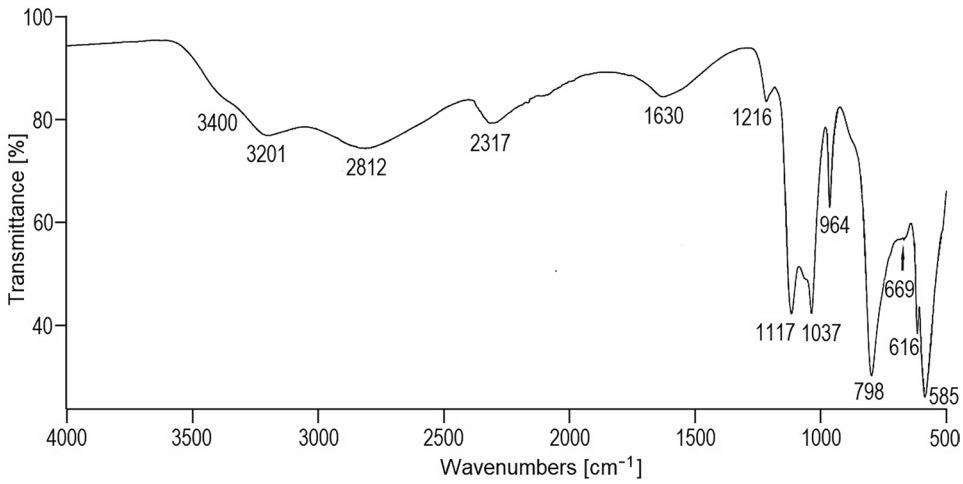

Fig. 2 IR spectrum of mallestigite

was obtained in the Rietveld refinement with a reflection half-width of 0.11° for the strongest peak. A minute peak of a small impurity of anglesite at $2\theta = 20.6°$ was neglected in the Rietveld refinement. It should be noted that the powder diffraction intensities are heavily dominated by Pb, Sb, As, and S due to their pseudosymmetric spatial arrangement, whereas O and H atoms play only a small role. Intensities and d values of the mallestigite X-ray powder pattern are presented in Table 1. Figure 3 includes also an X-ray powder pattern of fleischerite, $Pb_3Ge(SO_4)_2(OH)_6{\cdot}3H_2O$, hexagonal, $a = 8.867$ Å, $c = 10.875$ Å, calculated with the structural data of Otto (1975). A pronounced similarity to the pattern of mallestigite can be seen in the 2θ range 10 to 42°. However, the Bragg angles of fleischerite peaks are unmistakably shifted to higher values with increasing 2θ. It is worth mentioning that the similarity of mallestigite and fleischerite X-ray

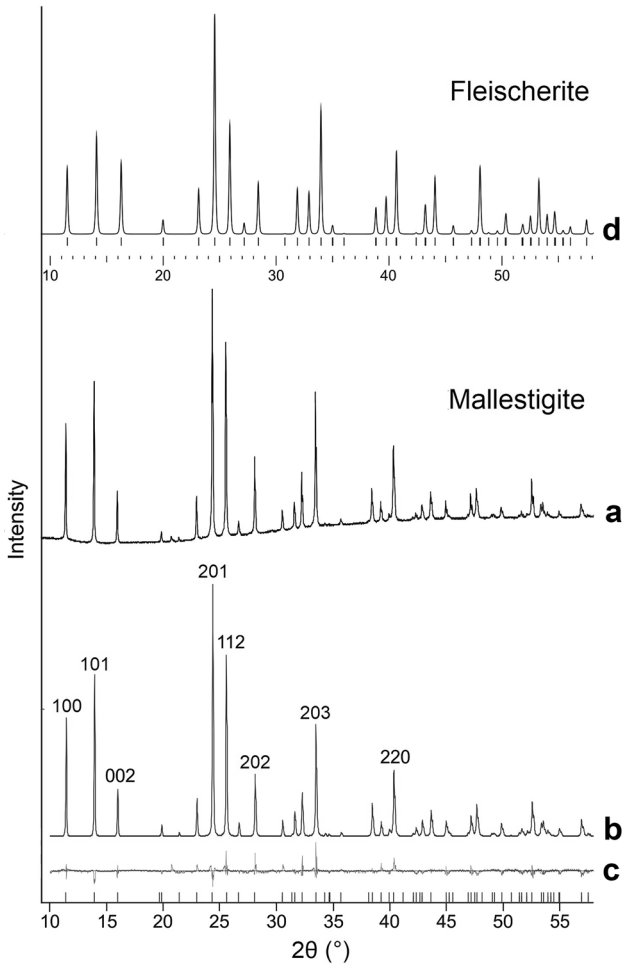

Fig. 3 X-ray powder pattern of mallestigite, $Pb_3Sb(SO_4)(AsO_4)(OH)_6{\cdot}3H_2O$, for Cu$K\alpha$ radiation: **a** as measured; **b** Rietveld fit to measured pattern without background and with the 8 strongest reflections indexed; **c** difference between measured and calculated pattern, $R_{wp} = 0.029$; **d** calculated X-ray powder pattern of fleischerite, $Pb_3Ge(SO_4)_2(OH)_6{\cdot}3H_2O$ (Otto 1975), shown for comparison

Table 1 X-ray powder diffraction data for mallestigite

I_{obs}	d_{obs}	d_{calc}	I_{calc}	$h\ k\ l$
47	7.7414	7.7359	33	1 0 0
65	6.3498	6.3474	55	1 0 1
21	5.5503	5.5522	18	0 0 2
4	4.4693	4.4663	4	1 1 0
1	4.1461	4.1437	1	1 1 1
17	3.8707	3.8679	13	2 0 0
100	3.6549	3.6527	100	2 0 1
78	3.4811	3.4801	84	1 1 2
5	3.3385	3.3389	6	1 0 3
31	3.1749	3.1737	27	2 0 2
8	2.9260	2.9239	6	1 2 0
11	2.8293	2.8275	5, 8	1 2 1, 2 1 1
23	2.7752	2.7761	23	0 0 4
55	2.6747	2.6742	63	2 0 3
2	2.5135	2.5118	3	3 0 1
14	2.3399	2.3387	20	3 0 2
8	2.2951	2.2944	4, 7	2 1 3, 1 2 3
30	2.2348	2.2331	42	2 2 0
3	2.1341	2.1347	6	1 0 5
6	2.1080	2.1066	2, 6	1 3 1, 3 1 1
11	2.0730	2.0718	16	2 2 2
7	2.0135	2.0132	7, 3	1 2 4, 2 1 4
10	1.9258	1.9260	17	2 0 5
12	1.9066	1.9053	19	4 0 1
1	1.8571	1.8562	2	1 3 3
1	1.8501	1.8507	2	0 0 6
4	1.8274	1.8263	8	4 0 2
16	1.7406	1.7400	33	2 2 4
5	1.7149	1.7141	11	0 4 3
6	1.7094	1.7098	9	1 1 6
2	1.6692	1.6695	5	2 0 6
5	1.6161	1.6151	7, 7	1 4 2, 4 1 2

I_{obs} and d_{obs} from Rietveld refinement using TOPAS 4.2

I_{calc} and d_{calc} calculated with data from single-crystal structure refinement

powder patterns did lead to misidentification, as happened for the type locality (Puttner 1995), and very likely for two reported fleischerite occurrences from deposits with Pb, Sb, As in sufficient amount but without Ge on the record (Dill et al. 1997; Navarro and Cardellach 2009).

Structure determination

Previous investigations by rotation and Weissenberg photographs of several crystals as well as a structure determination based on diffractometer data of a severely twinned crystal had shown that mallestigite is hexagonal and that it belongs to the fleischerite group (Sima et al. 1996; Sima

1998). However, the space group symmetry of the mineral, finally given as $P6_3$, and reliability of structural parameters remained open to question due to pseudosymmetry, twinning, and severe absorption.

For the present investigation a well-shaped hexagonal prism of nominal dimensions of $0.030\times0.036\times0.25$ mm^3 was investigated on a Bruker Smart APEX CCD diffractometer with graphite-monochromatized Mo$K\alpha$ radiation. After ascertaining that the crystal showed no superstructure or other detectable order-disorder effects, a total of 15,183 reflections covering a complete Ewald sphere up to $\theta_{max}=32°$ was collected by fine-sliced ω scans (0.3°, 30 s) in five hemicircle swings. After data integration with program SAINT (Bruker 2007), the reflection intensities were corrected for absorption by a combination of optimized analytic and multi-scan method using program SADABS (Bruker 2007). The hexagonal unit cell, $a=8.9326(4)$ and $c=11.1044(5)$ Å, determined by least-squares refinement of 7676 reflections in the θ range 2.6 − 31.7°, is in good agreement with the values extracted from X-ray powder diffraction. The analysis of the intensity data proved that the Laue symmetry is 6/*m* (Fig. 4) with 00 $l=2n+1$ as the only systematic extinction and a satisfactory R_{int} on merging symmetry equivalent reflections. This result corresponds with space groups $P6_3$ (non-centrosymmetric polar) and $P6_3/m$ (centrosymmetric) exclusively. Knowing from earlier investigations that mallestigite is closely related to fleischerite group minerals and their symmetry issues (see below), the crystal structure of mallestigite was assumed to be unknown and redetermined ab-initio using program SHELXT (Sheldrick 2015a) in multi-solution mode with all trigonal and hexagonal space groups considered. Space group $P6_3$ fared best among the 45 space groups evaluated followed by the hexagonal space groups $P\bar{6}$ and $P6_3/m$. Refinement of the fully ordered structure model in space group $P6_3$ with anisotropic displacement parameters for all atoms, a small inversion twinning parameter, and a correction for extinction led rapidly to $R1=0.0196$ (Sheldrick 2015b). At this stage a small orientation disorder of a sulfate oxygen atom was recognized that lowered $R1$ to 0.0186. Then the hydrogen atoms of the OH groups and the H_2O molecule were inferred from stereochemistry and were included in the refinement using the restraints O−H = 0.80 Å and H−O−H = 106° while their *x*,*y*,*z* were allowed to vary. In the final refinement $R1=0.0184$ for 1632 merged $F_o > 4\sigma(F_o)$ was obtained with a satisfactory agreement between F_o and F_c in all classes of reflections subdivided by F_o/F_{max} and resolution. The parameter for merohedral twinning on (001) refined to 0.07(1). A check of displacement ellipsoids, geometric data, and specific structural features was also satisfactory. The resulting crystallographic data are summarized in Table 2, and atomic parameters are given in Tables 3 and 4. A CIF with comments and unmerged reflection data is included in the supplementary materials. Structure graphics was generated with programs Diamond (Brandenburg 2016) and Mercury (Macrae et al. 2006).

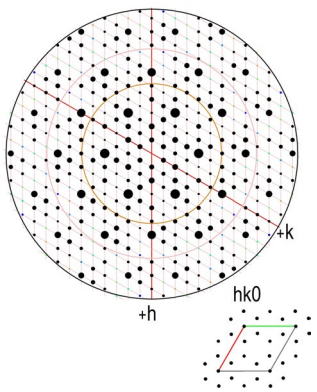

Fig. 4 *hk*0 layer of the weighted reciprocal lattice of mallestigite demonstrating the 6/*m* Laue symmetry. The largest spots −*hk*0 = 220, 600, 440, 820, 660 − reflect the two-dimensional pseudosymmetric arrangement of the heavy atoms Pb, Sb, and As in the unit cell shown on the lower right

Table 2 Crystal data and structure refinement for mallestigite

Chemical formula	$Pb_3Sb(SO_4)(AsO_4)(OH)_6{\cdot}3H_2O$
Formula weight	1134.40
Temperature	297(2) K
Wavelength	0.71073 Å
Crystal system	Hexagonal
Space group	$P6_3$
Unit-cell dimensions	$a=8.9326(4)$ Å
	$c=11.1044(5)$ Å
V	767.33(8) Å^3
Z	2
Mass density (calculated)	4.910 Mg/m^3
Absorption coefficient	36.92 mm^{-1}
$F(000)$	988
Crystal size	$0.030\times0.036\times0.25$ mm^3
θ range for data collection	2.63 to 31.97°
Index ranges	$-13\le h\le13$, $-13\le k\le13$, $-16\le l\le16$
Reflections collected	15,183
Independent reflections	1748 [$R_{int}=0.0297$]
Absorption correction	Analytical and multi-scan
Transmission	0.069 – 0.500
Refinement method	Full-matrix least-squares on F^2
Data / restraints / parameters	1748 (1632 with $I>2\sigma(I)$) / 6 / 88
Goodness-of-fit on F^2	1.051
Final R indices [$I>2\sigma(I)$]	$R1=0.0184$, $wR2=0.0414$
R indices (all data)	$R1=0.0206$, $wR2=0.0420$
Largest difference peak and hole	0.70 and −1.17 eÅ^{-3}

Table 3 Atomic coordinates and isotropic or equivalent isotropic displacement parameters (Å^2) for mallestigite

Atom	*x*	*y*	*z*	U_{eq}/U_{iso}
Pb	0.15901(2)	0.33705(2)	0.25623(10)	0.01847(8)
Sb	0	0	0[a]	0.00910(12)
S	1/3	2/3	0.0445(3)	0.0148(6)
As	1/3	2/3	0.49853(12)	0.0127(3)
O1	1/3	2/3	0.1799(8)	0.0182(16)
O2 [b]	0.1888(10)	0.5024(10)	0.0038(7)	0.036(2)
O2a [b]	0.308(7)	0.501(6)	0.003(4)	0.032(13)
O3	1/3	2/3	0.6476(8)	0.0170(17)
O4	0.2244(7)	0.4631(6)	0.4500(5)	0.0222(10)
O5h	0.2046(8)	0.1064(8)	0.1047(5)	0.0169(12)
O6h	0.1991(7)	0.1001(7)	0.3868(5)	0.0137(11)
O7w	0.5171(6)	0.4792(7)	0.2758(5)	0.0233(13)
H5h	0.288(5)	0.151(11)	0.062(5)	0.018
H6h	0.292(4)	0.139(11)	0.418(6)	0.018
H7wa	0.568(5)	0.449(6)	0.232(3)	0.028
H7wb	0.552(6)	0.480(9)	0.3422(14)	0.028

[a]origin fixing

[b]O2 and O2a are alternative sites of the SO_4 group with occupancies of 87(2) and 13(2)%, respectively

Discussion

The crystal structure of mallestigite

A general view of the crystal structure of mallestigite is shown in Fig. 5, closer details of the structure including bond lengths are outlined in Fig. 6 and Tables 5 and 6. The structure of mallestigite is built up from $[Sb^{5+}(OH)_6]^{1-}$ octahedra that are linked by triplets of edge-sharing Pb^{2+} to form infinite chains $\{Pb_3[Sb(OH)_6]\}^{5+}$ extending along 6_3 axes at 0,0,*z* parallel to the *c* axis. Each three of these chains are mutually linked via Pb-bonded SO_4^{2-} and AsO_4^{3-} anions located on 3-fold axes and three H_2O per formula unit around them. The SO_4^{2-} and AsO_4^{3-} anions alternate along the 3-fold axes and point with their apex atoms O1 and O3 all in the same direction making the structure clearly polar.

The pentavalent Sb atom is located on the 6_3 axis at 0,0,*z* and 0,0,*z*+½ with *z* = 0 fixed arbitrarily but not by symmetry requirements. It is in a distorted octahedral coordination by each three hydroxyl oxygen atoms O5h and O6h with Sb–O bond lengths of 1.964(6) and 1.988(6) Å, giving a mean value <Sb–O> = 1.976 Å, that is identical with the grand mean value reported for 158 $Sb^{5+}O_6$ octahedra (Gagné and Hawthorne 2018a). The edge lengths of this octahedron – O5h–O5h = 2.74 Å, O6h–O6h = 2.67 Å, O5h–O6h = 2.87 and 2.90 Å – show that it is distorted and stretched along the *c* axis. The distances between Sb and the two triangular faces of O5h and O6h are 1.16 and 1.26 Å, respectively. They and the Sb–O bond distances point to an asymmetry that is rooted in the Pb^{2+} atoms.

Pb^{2+} is located by 0.069 Å above *z* = ¼ and 0.085 Å off the (110) plane. It has a distinctly asymmetric coordination figure by four OH oxygen atoms, one sulfate oxygen O1, one arsenate oxygen O4 and two H_2O oxygen atoms O7w, which can be described to define a very distorted square antiprism with 2 O5h + 2 O6h and O1 + O4 + 2 O7w as the two square faces. This coordination figure is supplemented by O2 at a distinctly longer Pb–O distance (3.117 Å) to give a [9]-coordination with a Pb–O mean bond length of 2.743 Å. By far the strongest bond is to O4 of the AsO_4^{3-} group, Pb–O4 = 2.363 Å. It corresponds to a bond valence of 0.47 *vu* (*vu* are valence units calculated according to Gagné and Hawthorne 2015). Five Pb–O bonds with bond distances of 2.66–2.80 Å and bond valences of 0.24 to 0.18 *vu* (O6h, O7w, O1, O6h, O7w) subtend with the short bond Pb–O4 angles below 90° (O4–Pb–O = 76–84°) to give an umbrella-like arrangement. The remaining three oxygen ligands of Pb, two O5h and one O2, have longer Pb–O bonds (2.82, 2.84 and 3.12 Å, respectively) and subtend with the Pb–O4 bond angles between 130 and 145°. This demonstrates clearly that Pb is in a one-sided coordination figure and that the formal electron lone pair of Pb^{2+} is stereochemically active (Gagné and Hawthorne 2018a). In correspondence with this one-sidedness are the bonds Sb–O5h in the $Sb(OH)_6$ octahedron by 0.024 Å shorter than Sb–O6h.

The tetrahedral anions SO_4^{2-} and AsO_4^{3-} adopt distinctly different functions in the structure with Pb–O and hydrogen bonds selective for each group leading to their alternating arrangement along the 3-fold axis. The AsO_4^{3-} group is anchored by the three strong Pb–O4 bonds (2.363 Å), each supplemented by the short hydrogen bond O5h–H5···O4 (O5h···O4 = 2.64 Å) providing O4 with a bond strength of 0.47 + 0.26 = 0.73 *vu* that combines well with the 1.25 *vu* for the As–O bond of an ideal AsO_4^{3-} tetrahedron. The oxygen O4 lies nearly exactly in the plane Pb–As–O3 (deviation 0.011 Å) and keeps thereby the bond distances Pb–O4 and O5h···O4 to a minimum. The apical oxygen O3 is not bonded to Pb but accepts three short hydrogen bonds from H_2O7w, O7w···O3 = 2.69 Å. The As–O mean bond length, 1.663 Å, may be compared with grand mean distance of 1.687(27) Å for 508 AsO_4 tetrahedra (Gagné and Hawthorne 2018a).

The SO_4^{2-} group has a mean bond length of 1.470 Å in good agreement with <S–O> = 1.473 Å (Gagné and Hawthorne 2018b) for many sulfates. It is anchored in the structure by the apical oxygen O1 which is bonded to three Pb at Pb–O1 = 2.69 Å, corresponding to a bond strength of 3 × 0.23 = 0.69 *vu* that fits to the long bond S–O1 = 1.503 Å. Its basal oxygen O2 is weakly bonded to Pb and accepts a short hydrogen bond from O6h and a longer one from water O7w (Fig. 6). At variance with O4 of AsO_4^{3-} the sulfate oxygen O2 does not lie on the plane Pb–S–O1 in order to

Table 4 Atomic displacement parameters (Å^2) for mallestigite

	U_{11}	U_{22}	U_{33}	U_{23}	U_{13}	U_{12}
Pb	0.02109(12)	0.01482(11)	0.01702(12)	-0.00072(15)	-0.00047(18)	0.00711(8)
Sb	0.00969(14)	0.00969(14)	0.0079(2)	0	0	0.00485(7)
S	0.0140(9)	0.0140(9)	0.0165(14)	0	0	0.0070(5)
As	0.0123(4)	0.0123(4)	0.0136(6)	0	0	0.00615(18)
O1	0.019(2)	0.019(2)	0.017	0	0	0.0095(12)
O2	0.033(4)	0.027(4)	0.037(4)	-0.017(3)	-0.007(3)	0.008(3)
O3	0.021(3)	0.021(3)	0.009(3)	0	0	0.0104(14)
O4	0.029(3)	0.014(2)	0.016(2)	-0.0008(18)	0.001(2)	0.005(2)
O5h	0.011(3)	0.021(3)	0.015(2)	0.000(2)	-0.001(2)	0.006(2)
O6h	0.009(2)	0.016(2)	0.012(2)	0.0007(19)	0.0014(19)	0.004(2)
O7w	0.025(2)	0.029(2)	0.023(4)	-0.001(2)	0.0016(19)	0.018(2)

minimize Pb–O2, but is off from this plane by 0.52 Å [0.56 Å from (110)]. The cause for this position must sought in the hydrogen bond O7w···O2 = 2.903 Å, which would become overly long otherwise. The same feature can be seen for the Ba-Sn-Se compound addressed below. According to the refinement, about 13(2)% of oxygen O2 adopt a mirror-related position O2a (not shown in the Figures for clearness). This has similar bond distances to S, Pb, O6h, and O7w (1.45(5), 3.14, 2.72, 2.93 Å, respectively), very much like the main site but still probably requiring only a minute adjustment in the orientation of H_2O7w.

The hydroxyl groups O5h–H5h and O6h–H6h adopt similar triangular pyramidal coordination figures by Sb and two Pb atoms. Their approximate hydrogen atom positions are, therefore, geometrically predetermined. However, they could also be refined with the X-ray data using O–H distance restraints. Both groups form essentially straight hydrogen bonds of average strength (0.26 and 0.21 *vu* according to Ferraris and Ivaldi 1988), to O4 and O2 as H-bond acceptors (Table 6). Water H7wa–O7w–H7wb is in a distorted tetrahedral environment by two Pb and the H-bond acceptors O3 and O2 with tetrahedral angles of 95–122° about O7w. Interestingly, the two Pb–O7w bonds differ by 0.13 Å. Forcing the two Pb–O7w bonds in a trial least-squares refinement to become equal in length led to a significant increase in *R* values and, thus, was not supported by the diffraction data. Three O7w and three Pb form a 6-membered puckered ring (Fig. 6) with O7w by 0.22 Å above the mean plane of the three Pb atoms. With this arrangement the contact distances of O7w(x,y,z) to O1(x,y,z), O4(x,y,z), and O4(1-y,1+x-y,z) in the $Pb_3(O1)(O4)_3As(O7w)_3$ cage (Fig. 6, right side) are 3.06, 3.20, and 3.11 Å, respectively.

Pseudosymmetry

In the projection of the structure down [001] (Fig. 5b) one can easily note a significant pseudosymmetry with a near mirror symmetry on the plane (110). The atoms Sb, S, As, O1 and O3 are in special positions and located exactly on this pseudo-mirror plane. The remaining atoms – Pb, O5h, O6h, O2, O4, O7w and their H atoms – are in general positions. However, all of them – except the sulfate oxygen atom O2 – are very close to this pseudo-mirror plane. The specific deviations from plane (110) are in Å: Pb 0.085, O5h 0.037, O6h 0.005, O2 0.557, O4 0.064, O7w 0.017. Small as they are, these deviations are significant already in the (001) projection, but more so in 3 dimensions. Particularly the 0.085 Å deviation of Pb is highly significant and find its expression in the low Laue symmetry of the *hk*0 layer of the weighted reciprocal lattice shown in Fig. 4. Forcing Pb to lie exactly on the (110) plane would increase the *R*1 value from 0.0184 (Table 2) to ~0.15. However, it is not surprising that this pseudosymmetry facilitates merohedral twinning on (110) and this was a problem in earlier work (Sima et al. 1996; Sima 1998). Within the limits of detection, the high-quality crystal used in the present investigation was free of it. However, the crystal showed a modest 7(1)% merohedral twinning on (001). This reverses the polar axis of the structure and reverts the orientation of the SO_4 and AsO_4 tetrahedra upside down in parts of the crystal. A thorough check for diffuse or superstructure reflections of the investigated crystal showed no effects. Likewise, the X-ray powder patterns appeared clean and sharp. This indicates that the reversal is based on twinning and not on disorder.

Mallestigite and the fleischerite group

Mallestigite belongs to the group of minerals and synthetic compounds, which was named after fleischerite, $Pb_3Ge^{4+}(SO_4)_2(OH)_6{\cdot}3H_2O$, as its first known representative (Frondel and Strunz 1960). Based on their crystal structures this growing group can now be subdivided into three subgroups:

1. The minerals schaurteite, $Ca_3Ge^{4+}(SO_4)_2(OH)_6{\cdot}3H_2O$ (Origlieri and Downs 2013), genplesite, Ca_3Sn^{4+}

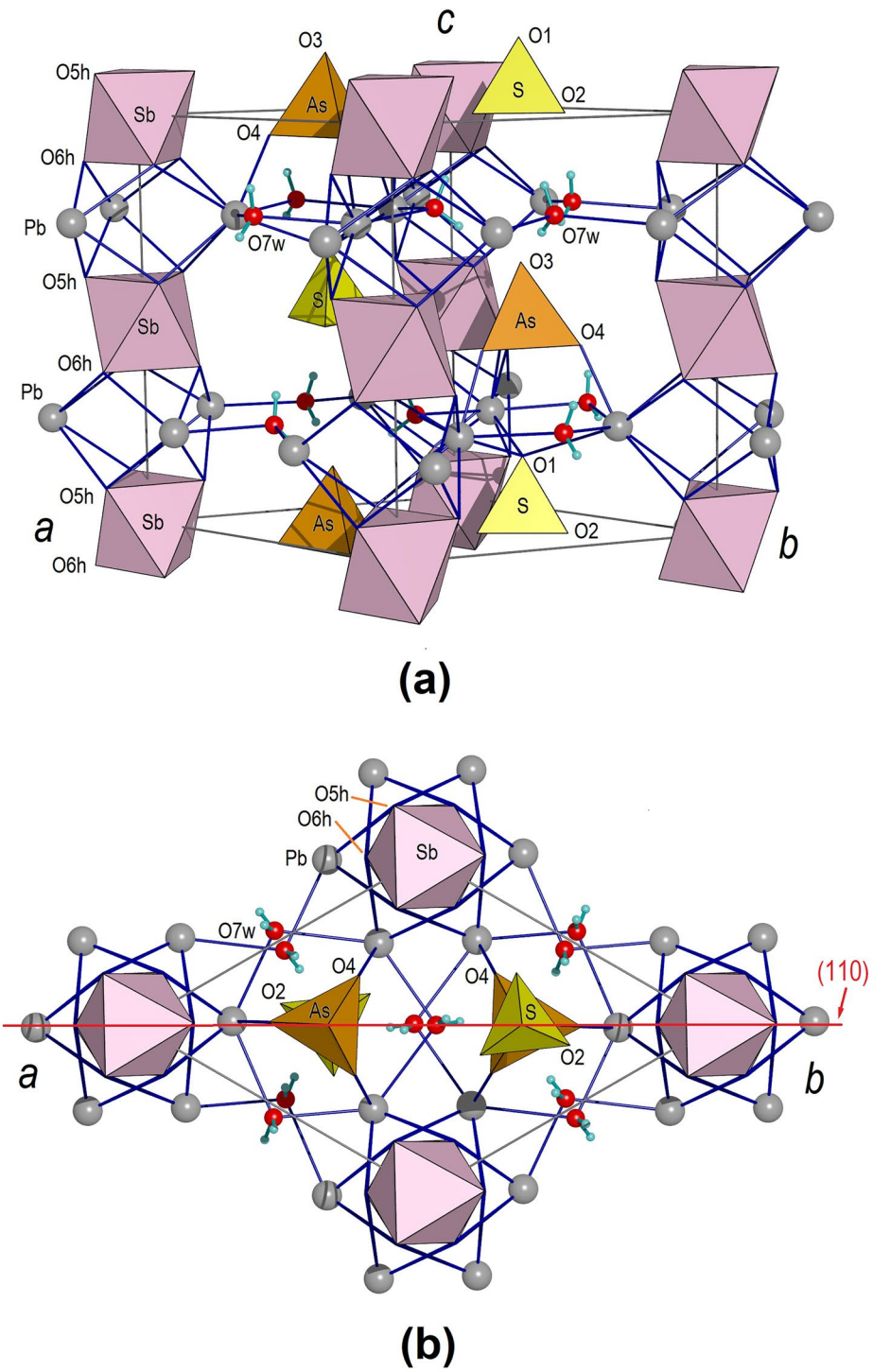

Fig. 5 The crystal structure of mallestigite, $Pb_3Sb(SO_4)(AsO_4)(OH)_6{\cdot}3H_2O$, in a general view (**a**), and in a projection along the *c* axis (**b**). 6_3 axes run along 0,0,*z* and 3-fold axes along $^1/_3,^2/_3,z$ and $^2/_3,^1/_3,z$. There are no other symmetry elements and the choice of origin with Sb in $z=0$ is arbitrary. H atoms of OH groups omitted. The structure is acentric polar with the upper vertices of the SO_4 and AsO_4 tetrahedra all pointing in the direction of the positive *c* axis. The red line in (**b**) represents the (110) plane to emphasize a pseudosymmetry that is outlined in the text

$(SO_4)_2(OH)_6{\cdot}3H_2O$ (Pekov et al. 2018), and despujolsite, $Ca_3Mn^{4+}(SO_4)_2(OH)_6{\cdot}3H_2O$ (Barkley et al. 2011).

2. The synthetic compound $Ba_3Sn^{4+}(SeO_4)_2(OH)_6{\cdot}3H_2O$ (Reuter and Kamaha 2022), mallestigite, $Pb_3Sb^{5+}(SO_4)(AsO_4)(OH)_6{\cdot}3H_2O$ (this work), and, probably, fleischerite $Pb_3Ge^{4+}(SO_4)_2(OH)_6{\cdot}3H_2O$ (Otto 1975).
3. Compounds with presently unknown status, namely synthetic $Sr_3Ge^{4+}(SO_4)_2(OH)_6{\cdot}3H_2O$ (Otto 1975) and a slag mineral with the tentative formula $Ba_3Sb^{5+}[(Si,S)O_3(OH)]_2(OH,O)_6{\cdot}3H_2O$ (Kolitsch et al. 2013).

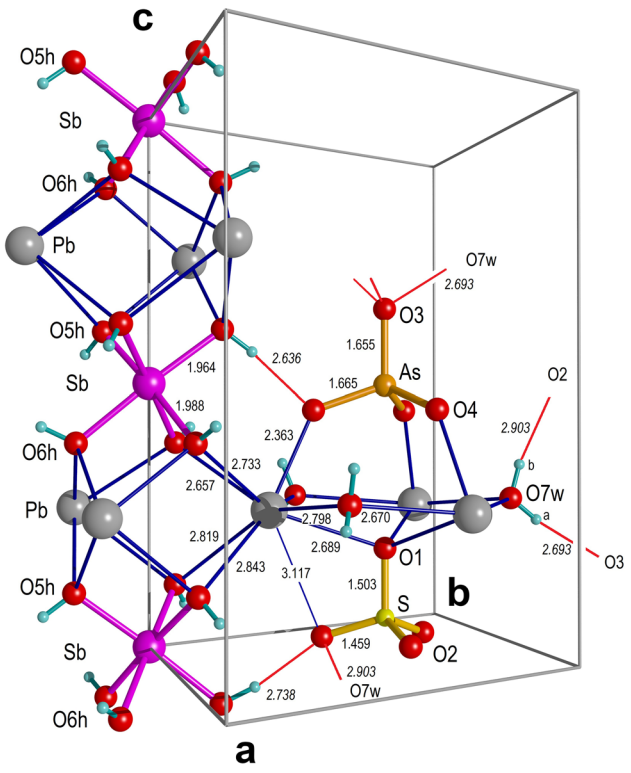

Fig. 6 Details of the crystal structure of mallestigite, $Pb_3Sb(SO_4)(AsO_4)(OH)_6{\cdot}3H_2O$, in ball-and-stick presentation with bond lengths in Å and H atoms in blue. Numbers in italics give O···O distances for hydrogen bonds

Table 5 Selected bond lengths and angles for mallestigite

Bond lengths [Å]		Bond angles (°)	
Pb-O4	2.363(5)		
Pb-O6h#1	2.657(5)		
Pb-O7w#7	2.670(5)		
Pb-O1	2.689(3)		
Pb-O6h	2.733(5)		
Pb-O7w	2.798(5)		
Pb-O5h#1	2.819(6)		
Pb-O5h	2.843(6)		
Pb-O2	3.117(8)		
<Pb-O>	2.743		
Sb-O5h#0,1,2 3×	1.964(6)	O5h-Sb-O5h 3×	88.6(3)
Sb-O6h#3,4,5 3×	1.988(6)	O6h-Sb-O6h 3×	84.3(3)
<Sb-O>	1.976	O5h-Sb-O6h 3×	92.9(3)
		O5h-Sb-O6h 3×	94.2(3)
		O5h-Sb-O6h 3×	176.9(3)
S-O1	1.503(9)	O1-S-O2 3×	108.0(3)
S-O2#0,6,7 3×	1.459(7)	O2-S-O2 3×	110.9(3)
<S-O>	1.470		
S-O2a#0,6,7 3×	1.45(5)		
As-O3	1.655(9)	O3-As-O4 3×	108.9(2)
As-O4#0,6,7 3×	1.665(5)	O4-As-O4 3×	110.1(2)
<As-O>	1.663		

Symmetry transformations used to generate equivalent atoms: #0 or none *x,y,z*; #1 *-y,x-y,z*; #2 *-x+y,-x,z*; #3 *-x,-y,z-½*; #4 *y,-x+y,z-½*; #5 *x-y,x,z-½*; #6 *1-y,1+x-y,z;* #7 *-x+y,1-x,z*

All members of the fleischerite group crystallize with hexagonal unit cells of $a \approx 9$ Å and $c \approx 11$ Å. They are built up from $M(OH)_6$ octahedra – $M = Mn^{4+}$, Ge^{4+}, Sn^{4+}, Sb^{5+} – linked by large divalent cations A (Ca, Sr, Ba, Pb) into infinite chains $A_3M(OH)_6$ which in turn are crosslinked by two tetrahedral anions (SO_4, SeO_4, AsO_4) and three H_2O per formula unit. A compilation of these compounds is given in Table 7.

Members of subgroup (1) crystallize in the centrosymmetric space group $P6_3/mmc$. They are at present exclusively based on Ca. They can be derived from mallestigite (Fig. 6) by inserting a center of inversion at $x,y,z = 0$, by adding a mirror plane parallel to (001) at $z = ¼$ and straightening out the Pb and H_2O layer, and by replacing the SO_4 tetrahedron with the (001) mirror image of the AsO_4 tetrahedron. By these means Ca becomes [8]-coordinated with a very regular square antiprism as coordination polyhedron; the OH groups of O5h and O6h become symmetry equivalent and donate hydrogen bonds to equivalents of O4 while the H_2O donate all hydrogen bonds to equivalents of O3 (Fig. 5a). Moreover, the (110) plane drawn in Fig. 5b becomes a crystallographic mirror plane leading ultimately to the space group symmetry $P6_3/mmc$ with *all* atoms of the structure lying on (110). A view of the corresponding structure, here schaurteite, is shown in Fig. 7a. Despujolsite, $Ca_3Mn^{4+}(SO_4)_2(OH)_6{\cdot}3H_2O$ (Barkley et al. 2011), as the only member of this subgroup reported to crystallize with a different space group, namely $P\bar{6}2c$, is so close to $P6_3/mmc$ symmetry, that it was assumed to adopt this space group. This assumption could be verified by a re-refinement with the published reflection data (Barkley et al. 2011) in space group $P6_3/mmc$ that improved previous $R1$ from 0.0235 ($P\bar{6}2c$) to 0.0196 ($P6_3/mmc$). For further details see supplementary materials.

Two members of subgroup (2) can be compared in Fig. 7b, c. Apart from mallestigite (Fig. 7b), what appears to be most interesting is the recently published and very well

Table 6 Hydrogen bonds for mallestigite [Å and °]

D-H···A	d(D-H)	d(H···A)	d(D···A)	∠(DHA)
O5h-H5h···O4#1	0.80	1.840(12)	2.636(8)	173(7)
O6h-H6h···O2#2	0.80	1.98(4)	2.738(9)	157(9)
O7w-H7wa···O3#3	0.80	1.905(12)	2.693(7)	168(5)
O7w-H7wb···O2#2	0.80	2.23(4)	2.903(10)	142(6)

X-ray hydrogen atom positions have been refined with hard restraints O-H = 0.80 Å for OH and H_2O, and H-O-H = 106° for H_2O. Symmetry transformations used to generate equivalent atoms are: #1 *y,-x+y,z-½*; #2 *y,-x+y,z+½*; #3 *1-x,1-y,z-½*

Table 7 Comparison of fleischerite type crystal structures, $A^{[8-9]}{}_3M^{[6]}(T^{[4]}O_4)_2(OH)_6{\cdot}3H_2O$, A^{2+} = Ca,Ba,Pb; M = Mn^{4+},Ge^{4+},Sn^{4+},Sb^{5+}; T = S^{6+},Se^{6+},As^{5+}

Name	Schaurteite	Genplesite	Despujolsite	Mallestigite	Synthetic	Fleischerite
Chemical formula	$Ca_3Ge(SO_4)_2(OH)_6{\cdot}3H_2O$	$Ca_3Sn(SO_4)_2(OH)_6{\cdot}3H_2O$	$Ca_3Mn(SO_4)_2(OH)_6{\cdot}3H_2O$	$Pb_3Sb(SO_4)(AsO_4)(OH)_6{\cdot}3H_2O$	$Ba_3Sn(SeO_4)_2(OH)_6{\cdot}3H_2O$	$Pb_3Ge(SO_4)_2(OH)_6{\cdot}3H_2O$
a [Å]	8.5253(4)	8.5139(2)	8.5405(5)	8.9326(4)	9.2550(6)	8.867(1)
c [Å]	10.8039(6)	11.1408(3)	10.8094(9)	11.1044(5)	11.4441(8)	10.875(1)
V [Å^3]	680.03(6)	699.37(3)	682.81(10)	767.33(8)	848.92(13)	740.5(2)
Space group	$P6_3/mmc$	$P6_3/mmc$	$P6_3/mmc$	$P6_3$	$P6_3$	$P6_3$
$R1$, reflections	0.0219, 456	0.0162, 590	0.0196, 450	0.0184, 1632	0.0083, 1653	0.036, 319
A^{2+}, c.n.	Ca, 8	Ca, 8	Ca, 8	Pb, 9	Ba, 9	Pb, 9
A^{2+}–O range [Å]	2.340–2.628	2.354–2.616	2.347–2.633	2.363–3.117	2.714–3.106	2.59–2.99
A^{2+}–O mean [Å]	2.487	2.489	2.488	2.743	2.837	2.72
$M^{4+/5+}$, c.n.	Ge^{4+}, 6	Sn^{4+}, 6	Mn^{4+}, 6	Sb^{5+}, 6	Sn^{4+}, 6	Ge^{4+}, 6
M–O mean [Å]	1.895	2.048	1.915	1.976	2.053	1.895
$T1$	S	S	S	S	Se	S
$T1$–O mean [Å]	1.468	1.472	1.472	1.470	1.636	1.48
$T2$				As	Se	S
$T2$–O mean [Å]				1.663	1.639	1.48
Reference	Origlieri and Downs (2013)	Pekov et al. (2018)	Barkley et al. (2011), recalculated*	Present work	Reuter and Kamaha (2022)	Otto (1975), modified**

$R1$, reflections – the crystallographic reliability index $R1$ and the number of reflections on which it is based

c.n. – coordination number

*This structure, previously reported in space group $P\bar{6}2c$, was reinterpreted in space group $P6_3/mmc$ and refined with the deposited diffraction data of Barkley et al. (2011). See supplementary materials for further details

**This structure of synthetic fleischerite, previously refined in space group $P\bar{6}2c$ with a disorder model (Otto 1975), was reinterpreted with an ordered mallestigite-like structure model in space group $P6_3$ using the published reflection data of Otto (1975). See supplementary materials for further details

refined crystal structure of $Ba_3Sn^{4+}(SeO_4)_2(OH)_6{\cdot}3H_2O$, a = 9.2550(6), c = 11.4441(8) Å, T = 100 K, $R1$ = 0.008 for 1653 reflections (Reuter and Kamaha 2022) presented in Fig. 7c. Like mallestigite, it adopts space group $P6_3$ and has the same architectural features, particularly the unidirectionally oriented two independent SeO_4^{2-} groups. With Ba^{2+} as a closed shell cation, a comparison with Pb^{2+} in mallestigite is of particular interest. For this purpose, the published structure (Reuter and Kamaha 2022) was transformed to mallestigite setting and its atoms relabeled (Fig. 7c). A list with crystallographic data of the transformed structure is provided in the supplementary materials. The SnO_6 octahedron, which has a mean bond length of 2.053 Å, is more regular than the SbO_6 octahedron in mallestigite, but shares with it an elongation along c axis. The SeO_4 tetrahedra (mean bond lengths 1.637 and 1.639 Å) are similar in size like the AsO_4 group in mallestigite and bigger than SO_4. Ba–O mean bond length is 2.837 Å, compared to Pb–O in mallestigite 2.743 Å. While the ionic radius of Ba^{2+} is only by about 0.1 Å bigger than that of Pb^{2+}, it is most significant that Ba–O4 = 2.714 Å is by ~0.35 Å longer than the corresponding short bond Pb–O4 = 2.363 Å in mallestigite. The two Ba–O6h bonds are ~0.06 Å longer and the two Ba–O5h bonds ~0.04 Å shorter than their counterparts in mallestigite (range for Ba 2.74–2.78 Å, for Pb 2.66–2.84 Å). Both Ba–O7w bonds are notably longer (on average by ~0.17 Å) than the two Pb–O7w bonds in mallestigite but differ less in length. The only bond that remains nearly unchanged is Ba–O2 = 3.11 Å compared with Pb–O2 = 3.12 Å. These features attest clearly that the observed asymmetry of the Pb^{2+} coordination in mallestigite is due to the lone pair effect.

The crystal structure of fleischerite, $Pb_3Ge^{4+}(SO_4)_2(OH)_6{\cdot}3H_2O$ (Otto 1975), the namesake mineral of the group was investigated by photographic X-ray methods using Cu$K\alpha$ radiation. The quality of natural material was so poor that a thin synthetic crystal was used for structure determination with multi-layer Weissenberg photographs. The Laue symmetry of this crystal was claimed as 6/*mmm* and a nearly centrosymmetric structure model in the acentric space group $P\bar{6}2c$ was worked out and refined to $R1$ = 0.039 for 319 reflections (Otto 1975). This structure model included an upside-down orientation disorder for the SO_4 groups which represents in principle a mallestigite type structure with a 1:1 twinning on (001) at z = ¼. Having experienced comparable features

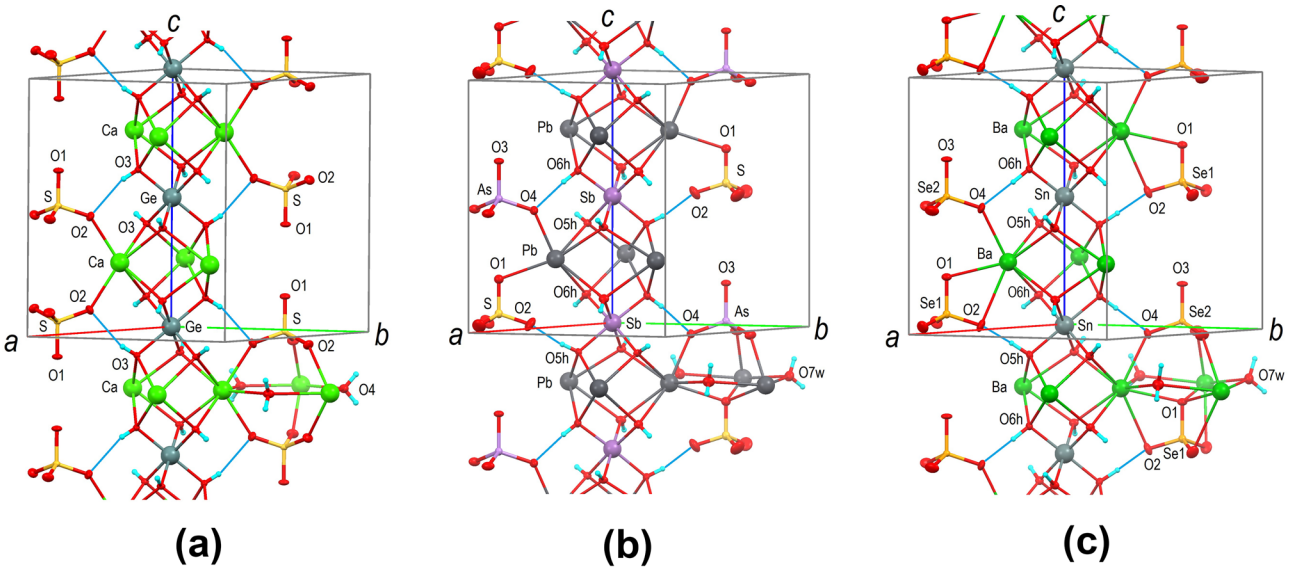

Fig. 7 Comparison of the crystal structures of **a** schaurteite, **b** mallestigite, and **c** $Ba_3Sn^{4+}(SeO_4)_2(OH)_6{\cdot}3H_2O$ (atoms relabeled and repositioned) using displacement ellipsoid presentation for oxygen atoms and the tetrahedral centers. Pb–O2 bond (3.12 Å) in (**b**) not shown. H bonds are thin blue lines

in earlier work on mallestigite (Sima et al. 1996; Sima 1998) and under consideration that Pb^{2+} should show a likewise coordination asymmetry, it is plausible to assume that fleischerite crystallizes in a mallestigite type structure with space group $P6_3$ and a corresponding ordered arrangement of the SO_4 tetrahedra, a possibility that was already considered by Otto (1975) albeit invoking space group $P31c$ as an alternative. Thus, Fig. 7b can be considered as an image of the fleischerite structure, when AsO_4 is replaced by a smaller SO_4 group. In order to test this hypothesis, the published diffraction data of Otto (1975) for fleischerite were used in a least-squares refinement with a mallestigite type structure. Starting with $R1 = 0.042$ (structure model of Otto in space group $P\bar{6}2c$) this refinement in space group $P6_3$ improved the reliability index to $R1 = 0.036$. It generated a notably asymmetric coordination for Pb (Pb–O4 = 2.59(2) Å, Pb–O2 = 2.99(2) Å; for atom designations see Fig. 6), and showed that the H_2O oxygen atom O7w is by 0.32 Å above the plane of the adjacent three Pb atoms. These results provide substantial support for a $P6_3$ symmetry of fleischerite. For further details see the supplementary materials.

Fleischerite subgroup (3) of unknown status comprises at present two compounds: For synthetic $Sr_3Ge^{4+}(SO_4)_2(OH)_6{\cdot}3H_2O$ only unit cell dimensions are known (Otto 1975). They are $a = 8.837(4)$, $c = 10.863(7)$ Å, similar to fleischerite and notably bigger than for schaurteite. As Sr^{2+} is frequently found in well-balanced [8]-coordination, a $P6_3/mmc$ type structure like schaurteite seems more likely than a $P6_3$ structure like the Ba-Sn selenate. Of the slag mineral $Ba_3Sb^{5+}[(Si,S)O_3(OH)]_2(OH,O)_6{\cdot}3H_2O$ (Kolitsch et al. 2013) only unit cell dimensions, $a = 8.810(1)$, $c = 11.776(2)$ Å, and the assigned space group $P\bar{3}$ were reported. Comparing the unit cell data with those of mallestigite and the synthetic Ba-Sn selenate, then a axis is shorter and c axis longer than one would expect for the given chemistry.

Further structural relationships

A short review on secondary antimony minerals was given by Roper et al. (2012). They typically form by oxidation of primary sulfides in the supergene zones of Sb-bearing ores and their mine wastes and they comprise a considerable variety of Sb^{5+} as well as Sb^{3+} oxygen compounds. One intermediate in their formation is the $[Sb(OH)_6]^{1-}$ complex. This is stable in near neutral to alkalic waters from which simple salt-like compounds crystallize, e.g. mopungite, $Na[Sb(OH)_6]$, a hydroxide-perovskite of tetragonal symmetry belonging to the stottite family (Bittarello et al. 2015), or brandholzite, $Mg[Sb(OH)_6]_2{\cdot}6H_2O$ (Friedrich et al. 2000), the representative of a family with a layered arrangement of $M^{2+}(H_2O)_6$, M = Mg, Ni, Co, and $Sb(OH)_6$ octahedra crosslinked by hydrogen bonds (Bonazzi and Mazzi 1996; Friedrich et al. 2003).

A large group of minerals with close structural relationships to the fleischerite family is represented by thaumasite, $Ca_3Si^{4+}(CO_3)(SO_4)(OH)_6{\cdot}12H_2O$, and ettringite, $Ca_3Al^{3+}(SO_4)_{1.5}(OH)_6{\cdot}{\sim}13H_2O$, as prototypes (Taylor 1973). These minerals are based on the same $A_3M(OH)_6$ chains like the fleischerite group. One particular example is that with schaurteite $Ca_3Ge^{4+}(OH)_6$ chains. On virtual transition from schaurteite to thaumasite, Ge^{4+} in octahedral coordination is replaced by Si^{4+} while the bridging water molecules and the sulfate O atoms bonded to Ca are substituted by four terminal H_2O. This leads to

completely hydrated cationic columns $[Ca_3M^{4+}(OH)_6(H_2O)_{12}]^{4+}$ with 30 active H atoms per formula unit, of which 6 hydroxyl and 3 aquo H atoms are strengthening the columns by internal hydrogen bonds, whereas 21 H atoms are available for external hydrogen bonds to suitable anions. These columns have inherent 6_3 symmetry and adopt hexagonal rod-packing with interstitial space of trigonal symmetry. They, therefore, tend to adopt anions with suitable symmetry, size, charge and H-bonding propensity, SO_4^{2-} and CO_3^{2-} in case of thaumasite and $P6_3$ space group symmetry with $a \approx 11.0$, $c \approx 10.4$ Å (Edge and Taylor 1971; Gatta et al. 2012). In the mineral realm, examples with tetravalent M=Si^{4+}, Ge^{4+}, Mn^{4+} and anions like SO_4^{2-}, CrO_4^{2-}, CO_3^{2-}, SO_3^{2-} or combinations thereof are known. If M is trivalent, like Al^{3+}, Fe^{3+}, Cr^{3+}, then the polyhedral columns have a lower net charge $[Ca_3M^{3+}(OH)_6(H_2O)_{12}]^{3+}$. This seems to lead to complications with anion incorporation, additional water molecules, disorder, and a doubling of the c axis, as revealed in a recent neutron diffraction study of an ettringite with the chemical formula $Ca_6Al_2(SO_4)_3(OH)_{12}{\cdot}27H_2O$ (Gatta et al. 2019). The formal hydration of schaurteite $[Ca_3Ge(OH)_6]^{4+}$ chains is possible, as demonstrated by the existence of carraraite, $Ca_3Ge^{4+}(CO_3)(SO_4)(OH)_6{\cdot}12H_2O$ (Merlino and Orlandi 2001). However, it is unlikely that the higher charged $[Pb_3Sb(OH)_6]^{5+}$ chain in mallestigite with Pb^{2+} as a more polarizable cation might form a stable thaumasite/ettringite type chain with $Pb(OH)_4(H_2O)_4$ polyhedra.

Concluding remarks

Mallestigite is a secondary mineral with an interesting crystal chemistry. The modes of its formation under laboratory conditions, its solubility and its thermodynamic stability will have to be explored in the future. Present knowledge shows that the crystal structure of mallestigite is embedded in two related structural families of which one, the thaumasite/ettringite family, is widespread and abundant. This points to a notable stability of these minerals and their backbone, in case of mallestigite the $[Pb_3Sb^{5+}(OH)_6]^{5+}$ chains, and consequently to a certain propensity of their formation. When, under humid oxidizing conditions, galena and fahlores of the tetrahedrite-tennantite series or complex Pb-As-Sb-sulfosalts are present as primary minerals and sources for Pb^{2+}, Sb^{5+}, AsO_4^{3-}, and SO_4^{2-}, then good chances for the formation of mallestigite as supergene mineral are given, as exemplified by the type locality on Mallestiger Mittagskogel and the four presently known further occurences (see introduction). Stockpiled wastes from metal mining and metal extraction with Pb, Sb and As in significant concentrations are widespread (Wilson et al. 2010; Okkenhaug et al. 2011 and references therein). Hence, it is expected that the number of mallestigite occurrences will significantly grow in number if appropriate methods in the identification of the mineral are at hand. Two prospective locations have been highlighted in the chapter X-ray powder diffraction. As a long time sink for the toxic heavy metals Pb, Sb, As the mineral mallestigite is likely not sufficiently stable. Here phases of the alunite/jarosite supergroup like beudantite, $PbFe_3(SO_4)(AsO_4)(OH)_6$, and relatives are certainly more stable and have been shown that they may incorporate significant amounts of Sb^{5+} in octahedral coordination as replacement for Fe^{3+} (Kolitsch et al. 1999; Mills et al. 2014; Pekov et al. 2016). In case of the mallestigite type locality, iron does not play a major role and jarosite was there found only as a very rare species.

Supplementary Information The online version contains supplementary material available at https://doi.org/10.1007/s00710-023-00837-y.

Acknowledgements We dedicate this article to the memory of Prof. Dr. Josef Zemann (1923–2022), an inspiring teacher and scientist. The X-ray center of Technical University Wien is acknowledged for providing access to the single-crystal X-ray diffractometer. We are grateful for discussions and technical support by Christian Auer, Leopold Weber, and Thomas Hofmann of the Geosphere Austria (the Geological Survey of Austria, formerly Geologische Bundesanstalt) and for insights provided by Karl Krainer, Innsbruck. Nandini Venkata provided linguistic support. We thank Igor V. Pekov and an anonymous reviewer as well as Guest Editor Luca Bindi and Chief Editor Lutz Nasdala for their constructive suggestions and help.

Funding Open access funding provided by Technical University Wien (TUW).

References

Barkley MC, Yang H, Evans SH, Downs RT, Origlieri MJ (2011) Redetermination of despujolsite, $Ca_3Mn^{4+}(SO_4)_2(OH)_6{\cdot}3H_2O$. Acta Crystallogr E67:i47–i48

Bittarello E, Camara F, Ciriotti ME, Marengo A (2015) Ottensite, brizziite and mopungite from Pereta mine (Tuscany, Italy): new occurrences and crystal structure refinement of mopungite. Min Petrol 109:431–442

Bonazzi P, Mazzi F (1996) Bottinoite, $Ni(H_2O)_6[Sb(OH)_6]_2$: crystal structure, twinning, and hydrogen bond model. Am Mineral 81:1494–1500

Brandenburg K (2016) Diamond (Version 4.0). Crystal and Molecular Structure Visualization

Bruker (2007) Programs SMART, SAINT, and SADABS. Bruker AXS Inc., Madison, Wisconsin, USA

Bruker (2009) TOPAS Software user Manual Version 4.2. Bruker AXS Inc., Madison, Wisconsin, USA

Canaval R (1926) Bemerkungen über die Erzvorkommen in der Umgebung von Finkenstein bei Villach. Mont Rundschau 18:179–184

Chukanov NV (2014) Infrared spectra of mineral species. Extended library volume 2. Springer, Dordrecht

Dill HG, Pertold Z, Riera Kilibarda C (1997) Sediment-hosted and volcanic-hosted Sb vein mineralization in the Potosi region, Central Bolivia. Economic Geol 92:623–632

Edge RA, Taylor HFW (1971) Crystal structure of Thaumasite, $[Ca_3Si(OH)_6{\cdot}12H_2O](SO_4)(CO_3)$. Acta Crystallogr B27:594–601

Ferraris G, Ivaldi G (1988) Bond valence vs bond length in O···O hydrogen bonds. Acta Crystallogr B44:341–344

Friedrich A, Wildner M, Tillmanns E, Merz PL (2000) Crystal chemistry of the new mineral brandholzite, $Mg(H_2O)_6[Sb(OH)_6]_2$, and of the synthetic analogues $M^{2+}(H_2O)_6[Sb(OH)_6]_2$ (M^{2+} = Mg, Co). Am Mineral 85:593–599

Friedrich A, Mazzi F, Wildner M, Tillmanns E (2003) Isotypism of $Co(H_2O)_6[Sb(OH)_6]_2$ with brandholzite and bottinoite. Am Mineral 88:462–463

Frondel C, Strunz H (1960) Fleischerit und Itoit, zwei neue Germanium-Mineralien von Tsumeb. Neues Jahrb Mineral Monatshefte 1960:132–142

Gagné OC, Hawthorne FC (2015) Comprehensive derivation of bond-valence parameters for ion pairs involving oxygen. Acta Crystallogr B71:562–578

Gagné OC, Hawthorne FC (2018a) Bond-length distributions for ions bonded to oxygen: metalloids and post-transition metals. Acta Crystallogr B74:63–78

Gagné OC, Hawthorne FC (2018b) Bond-length distributions for ions bonded to oxygen: results for the non-metals and discussion of lone-pair stereoactivity and the polymerization of PO_4. Acta Crystallogr B74:79–96

Gatta GD, McIntyre GJ, Swanson JG, Jacobsen SD (2012) Minerals in cement chemistry: a single-crystal neutron diffraction and Raman spectroscopic study of thaumasite, $Ca_3Si(OH)_6(CO_3)(SO_4){\cdot}12H_2O$. Am Mineral 97:1060–1069

Gatta GD, Hålenius U, Bosi F, Cañadillas-Delgado L, Fernandez-Diaz MT (2019) Minerals in cement chemistry: a single-crystal neutron diffraction study of ettringite, $Ca_6Al_2(SO_4)_3(OH)_{12}{\cdot}27H_2O$. Am Mineral 104:73–78

Giarduz M, Iob S, Bittarello E, Ciriotti M, Fassina B (2015) Mallestigite di Monte Avanza: terzo ritrovamento mondiale. Micro 2–2015:54–63

IRIS (2023) IRIS online – Interactive Raw Material Information System of the Geologic Survey of Austria (GBA – Geosphere Austria), https://www.geologie.ac.at/en/services/web-applications/interactiv-raw-material-information-system (last accessed 23 Mar 2023)

Kolitsch U, Slade PG, Tiekink ERT, Pring A (1999) The structure of antimonian dussertite and the role of antimony in oxysalt minerals. Min Mag 63:17–26

Kolitsch U, Brandstätter F, Schreiber F, Fink R, Auer C (2013) Die Mineralogie der weltweit einzigartigen Schlacken von Waitschach, Kärnten. Annalen des Naturhistorischen Museums in Wien Serie A 115:19–87

Macrae CF, Edgington PR, McCabe P, Pidcock E, Shields GP, Taylor R, Towler M, van de Streek J (2006) Mercury: visualization and analysis of crystal structures. J Appl Cryst 39:453–457

Merlino S, Orlandi P (2001) Carraraite and zaccagnaite, two new minerals from the Carrara marble quarries: their chemical compositions, physical properties, and structural features. Am Mineral 86:1293–1301

Mills SJ, Etschmann B, Kampf AR, Poirier G, Newville M (2014) Sb^{5+} and Sb^{3+} substitution in segnitite: a new sink for As and Sb in the environment and implications for acid mine drainage. Am Mineral 99:1355–1359

Navarro A, Cardellach E (2009) Mobilization of Ag, heavy metals and Eu from the waste deposit of the Las Herrerias mine (Almeria, SE Spain). Environ Geol 56:1389–1404

Okkenhaug G, Zhu Y-G, Luo L, Lei M, Li X, Mulder G (2011) Distribution, speciation and availability of antimony (Sb) in soils and terrestrial plants from an active Sb mining area. Environ Pollution 159:2427–2434

Origlieri MJ, Downs RT (2013) Schaurteite, $Ca_3Ge(SO_4)_2(OH)_6{\cdot}3H_2O$. Acta Crystallogr E69:i6

Otto HH (1975) Die Kristallstruktur von Fleischerit, $Pb_3Ge[(OH)_6|(SO_4)_2]{\cdot}3H_2O$, sowie kristallchemische Untersuchungen an isotypen Verbindungen. Neues Jahrb Mineral Abhandlungen 123:160–190

Pekov IV, Khanin DA, Yapaskurt VO, Pakunova AV, Ekimenkova IA (2016) Minerals of the beudantite–segnitite series from the oxidation zone of the Berezovskoe gold deposit, middle urals: Chemical variations, behavior of admixtures, and antimonian varieties. Geol Ore Deposits 58:600–611

Pekov IV, Sereda EV, Zubakova NV, Yapaskurt VO, Chukanov NV, Britvin SN, Lykova IS, Pushcharovsky DY (2018) Genplesite, $Ca_3Sn(SO_4)_2(OH)_6{\cdot}3H_2O$, a new mineral of the fleischerite group: first occurrence of a tin sulfate in nature. Eur J Mineral 30:375–382

Poeverlein R, Gröbner J (2007) Der Bergbau Geyer bei Rattenberg in Tirol und seine Mineralien. Lapis 32(2):34–39

Pouchou JL, Pichoir F (1991) Quantitative analysis of homogeneous or stratified microvolumes applying the model "PAP. In: Heinrich KFJ, Newbury DE (eds) Electron Probe quantification. Plenum Press, New York, pp 31–75

Puttner M (1994) Der Bergbau auf die Tetraedrit-Vorkommen des Mallestiger Mittagskogels (Westkarawanken, Kärnten), seine Bergbaugeschichte und Mineralogie sowie der Neufund von Clarait und Theisit. Aufschluss 45:1–10

Puttner M (1995) Neue Minerale vom Bergbau Neufinkenstein-Grabanz in Kärnten: Adamin, Anglesit, Bayldonit, Chalkophyllit, Fleischerit (?), Parnauit, Schultenit, Serpierit, Devillin, Strashimirit, Tirolit. Mineralogische Rundschau 2(1):17–22

Reuter H, Kamaha S (2022) $Ba_3Sn(SeO_4)_2(OH)_6{\cdot}3H_2O$, a hydrated 1:2 double salt of barium hexahydroxidostannate(IV) and barium selenate(VI). Acta Crystallogr E78:809–813

Rewitzer C, Hochleitner R, Fehr T (2020) Mina Casualidad, Baños de Alhamilla, Almería, Spain (part 2). Mineral Up 5(5):8–36

Roper AJ, William PA, Montserrat F (2012) Secondary antimony minerals: phases that control the dispersion of antimony in the supergene zone. Chem Erde 72(S4):9–14

Schnorrer G (2003) Mallestigit, $Pb_3Sb[(OH)_6|AsO_4|SO_4]{\cdot}3H_2O$, eine weitere Mineralneubildung in den antiken Schlacken des Harzes – ein zweiter Fundort für diese Verbindung und ein weiterer Beweis für die Bildung sowohl auf "natürlichen" als auch auf "künstlichen" Schlackenhalden. Aufschluss 54:42–44

Sheldrick GM (2015a) SHELXT – Integrated space-group and crystal-structure determination. Acta Crystallogr A71:3–8

Sheldrick GM (2015b) Crystal structure refinement with SHELXL. Acta Crystallogr C71:3–8

Sima I (1998) Mallestigit, $Pb_3Sb(SO_4)(AsO_4)(OH)_6{\cdot}3H_2O$, ein neues Mineral von einer Halde des ehemaligen Cu–Pb–Zn-Bergbaues NW des Mallestiger Mittagskogels in den Westkarawanken, Kärnten, Österreich. Mitteil Österr Mineral Ges 143:225–227

Sima I, Ettinger K, Koppelhuber-Bitschnau B, Taucher J, Walter F (1996) $Pb_3Sb(OH)_6(AsO_4,SO_4)_2{\cdot}3H_2O$, ein neues Mineral isotyp mit Fleischerit. Mitteil Österr Mineral Ges 141:224–225

Taucher J (1998) Über Erzminerale von der Grabanz, Neufinkenstein, Mallestiger Mittagskogel, Karawanken, Kärnten, Österreich sowie eine Richtigstellung zum Mallestigit. Carinthia II 188/189:377–392

Taylor HFW (1973) Crystal structures of some double hydroxide minerals. Mineral Mag 39:377–389

Walter F, Auer C, Bernhard F et al (2016) Neue Mineralfunde aus Österreich LXV. Carinthia II 206/126:203–250

Weber L (1997) Handbuch der Lagerstätten der Erze, Industrieminerale und Energierohstoffe Österreichs. Archiv für Lagerstättenforschung, p 19

Wilson SC, Lockwood PV, Ashley PM, Tighe M (2010) The chemistry and behaviour of antimony in the soil environment with comparisons to arsenic: a critical review. Environ Pollut 158:1169–1181